Monthly Notices of the ROYAL ASTRONOMICAL SOCIETY

MNRAS **477,** 491–506 (2018) doi:10.1093/mnras/sty670
Advance Access publication 2018 March 14

Cosmological constraints from galaxy clustering in the presence of massive neutrinos

M. Zennaro,[1,2]★ J. Bel,[2,3] J. Dossett,[2] C. Carbone[1,2,4] and L. Guzzo[1,2]

[1] *Università degli studi di Milano – Dipartimento di Fisica, via Celoria, 16, I-20133 Milano, Italy*
[2] *INAF – Osservatorio Astronomico di Brera, Via Brera, 28, I-20121 Milano, Italy*
[3] *Aix Marseille Univ, Université de Toulon, CNRS, CPT, F-13009, Marseille, France*
[4] *INFN – Sezione di Milano, via Celoria, 16, I-20133 Milano, Italy*

Accepted 2018 March 6. Received 2018 March 6; in original form 2017 December 7

ABSTRACT

The clustering ratio is defined as the ratio between the correlation function and the variance of the smoothed overdensity field. In Λ cold dark matter (ΛCDM) cosmologies without massive neutrinos, it has already been proven to be independent of bias and redshift space distortions on a range of linear scales. It therefore can provide us with a direct comparison of predictions (for matter in real space) against measurements (from galaxies in redshift space). In this paper we first extend the applicability of such properties to cosmologies that account for massive neutrinos, by performing tests against simulated data. We then investigate the constraining power of the clustering ratio on cosmological parameters such as the total neutrino mass and the equation of state of dark energy. We analyse the joint posterior distribution of the parameters that satisfy both measurements of the galaxy clustering ratio in the SDSS-DR12, and the angular power spectra of cosmic microwave background temperature and polarization anisotropies measured by the *Planck* satellite. We find the clustering ratio to be very sensitive to the CDM density parameter, but less sensitive to the total neutrino mass. We also forecast the constraining power the clustering ratio will achieve, predicting the amplitude of its errors with a Euclid-like galaxy survey. First we compute parameter forecasts using the *Planck* covariance matrix alone, then we add information from the clustering ratio. We find a significant improvement on the constraint of all considered parameters, and in particular an improvement of 40 per cent for the CDM density and 14 per cent for the total neutrino mass.

Key words: neutrinos – cosmological parameters – dark energy – large-scale structure of Universe.

1 INTRODUCTION

Present-time as well as forthcoming galaxy surveys, while on the one hand will allow us to reach unprecedented precision on the measurement of the galaxy clustering in the universe, on the other hand will challenge us to produce more accurate and reliable predictions. The effect of massive neutrinos on the clustering properties of galaxies, that in the past has been either neglected or considered as a nuisance parameter, is nowadays regarded as one of the key points to be included in the cosmological model in order for it to reach the required accuracy. At the same time, while allowing for more realistic predictions of cosmological observables, this process also helps in shedding light on some open issues of fundamental physics, such as the neutrino total mass or the hierarchy of their mass splitting.

From the experimental measurements of neutrino flavour oscillations, particle physics has been able to draw a constraint on the mass splitting of the massive eigenstates of neutrinos, and set a lower bound to the total neutrino mass, $M_\nu = \sum m_{\nu,i} \gtrsim 0.06$ eV at 95 per cent level (Gonzalez-Garcia et al. 2012; Forero, Tórtola & Valle 2014; Gonzalez-Garcia, Maltoni & Schwetz 2014; Esteban et al. 2017).

On the other hand, the absolute scale of magnitude of neutrino masses is still an open issue. Beta decay experiments such as the ones carried out in Mainz and Troitsk have set as an upper limit at 95 per cent level on the electron neutrino mass of $m(\nu_e) < 2.2$ eV (Kraus et al. 2005). While future experiments like Katrin project much higher sensitivities, on the order of 0.2 eV (Bonn et al. 2011), present-day cosmology can already intervene in the debate about neutrino mass.

Since neutrinos are light and weakly interacting, they decouple from the background when still relativistic. Therefore, even at late times they are characterized by large random velocities

★ E-mail: matteo.zennaro90@gmail.com

that prevent them from clustering on small scales. As a consequence, neutrinos introduce a characteristic scale-dependent and redshift-dependent suppression of the clustering, whose amplitude depends on the value of their mass. In fact, the presence of massive neutrinos influences the evolution of matter overdensities in the universe, depending on their mass. There have been a large number of works extensively studying the interplay between cosmology and neutrino physics (see, for instance, Lesgourgues & Pastor 2006, 2012, 2014, and references therein). Moreover, in addition to the many constraints already obtained with present-day cosmological data (see, for example, Cuesta, Niro & Verde 2016; Vagnozzi et al. 2017), future surveys prospect even more exciting results (Carbone et al. 2011b; Archidiacono et al. 2017).

As we aim to describe the clustering of galaxies in cosmologies with massive neutrinos, we have to cope with the description of the galaxy–matter bias. As a matter of fact, galaxies do not directly probe the matter distribution in the universe, being in fact a discrete sampling of its highest density peaks. We choose to describe galaxy clustering through a recently introduced observable that, on sufficiently large scales, does not depend on the galaxy–matter bias, the clustering ratio (Bel & Marinoni 2014).

In standard Λ cold dark matter (ΛCDM) cosmologies, this observable has already been proved to be a reliable cosmological probe for constraining cosmological parameters, being particularly sensitive to the amount of matter in the universe, as shown in Bel et al. (2014).

In this work we aim at studying how the clustering properties of galaxies are modified by the presence of neutrinos, and in particular we want to extend the clustering ratio approach to cosmologies including massive neutrinos. By proving that this observable maintains its properties, we want to exploit it to constrain the total neutrino mass.

This paper will be organized as follows. In Section 2 we will introduce the statistical observable we are going to use, the clustering ratio, and its properties. We will show why this observable can be considered unaffected either by the galaxy–matter bias on linear scales and redshift-space distortions, and we will introduce its estimators.

In Section 3 we will describe the effects of massive neutrinos on the matter and galaxy clustering. We will introduce the 'Dark Energy and Massive Neutrino Universe' (DEMNUni) simulations, the set of cosmological simulations we use to test the properties of the clustering ratio in a cosmology with massive neutrinos. Finally we will show that the properties of the clustering ratio hold as well in cosmologies that include massive neutrinos, in particular confirming the independence of the clustering ratio from bias and redshift-space distortions on linear scales in the DEMNUni simulations.

Section 4 is devoted to presenting our results. We use measurements of the clustering ratio in the Sloan Digital Sky Survey Data Release 7 and 12 to draw a constraint on the total neutrino mass and on the equation of state of dark energy. In particular we study the joint posterior distribution of the parameters of the model, including M_ν and w, obtained from the clustering ratio measurement and the latest cosmic microwave temperature and polarization anisotropy data from the *Planck* satellite.

2 CLUSTERING RATIO

In order to describe the statistical properties of the matter distribution in the universe, we use the overdensity field

$$\delta(\boldsymbol{x}, t) = \frac{\rho(\boldsymbol{x}, t)}{\bar{\rho}(t)} - 1, \tag{1}$$

where $\rho(\boldsymbol{x}, t)$ is the value of the matter density at each spatial position, while $\bar{\rho}(t)$ represents the mean density of the universe.

This is assumed to be a random field with null mean. Information on the distribution must therefore be sought in its higher order statistics, such as the variance $\sigma^2 = \langle \delta^2(\boldsymbol{x}) \rangle_c$ and the two-point autocorrelation function $\xi(r) = \langle \delta(\boldsymbol{x})\delta(\boldsymbol{x}+\boldsymbol{r}) \rangle_c$ of the field. Here $\langle \cdot \rangle_c$ denotes the cumulant moment, or connected expectation value (Fry 1984).

In this work we will always consider the matter distribution smoothed on a certain scale R by evaluating the density contrast in spherical cells, i.e.

$$\delta_R(\boldsymbol{x}) = \int \delta(\boldsymbol{x}') W\left(\frac{|\boldsymbol{x} - \boldsymbol{x}'|}{R}\right) \mathrm{d}^3\boldsymbol{x}', \tag{2}$$

where W is the spherical top-hat window function. As a consequence, the variance and correlation function will be smoothed on the same scale, and will be denoted σ_R^2 and $\xi_R(r)$.

An equivalent description of the statistical properties of the matter field can be obtained in Fourier space in terms of the matter power spectrum. Starting from the Fourier transform of the matter overdensity field,

$$\hat{\delta}(\boldsymbol{k}) = \int \frac{\mathrm{d}^3\boldsymbol{x}}{(2\pi)^3} \mathrm{e}^{-\mathrm{i}\boldsymbol{k}\cdot\boldsymbol{x}}\, \delta(\boldsymbol{x}), \tag{3}$$

the matter density power spectrum is defined according to

$$\langle \hat{\delta}(\boldsymbol{k}_1)\hat{\delta}(\boldsymbol{k}_2) \rangle = \delta^D(\boldsymbol{k}_1 + \boldsymbol{k}_2) P(\boldsymbol{k}_1), \tag{4}$$

while the adimensional power spectrum can be written as $\Delta^2(k) = 4\pi P(k) k^3$. The variance and correlation function of the matter field are linked to its power spectrum, representing in fact different ways of filtering it. The variance is the integral over all the modes, modulated by the Fourier transform of the filtering function $\hat{W}$,

$$\sigma_R^2 = \int_0^\infty \Delta^2(k) \hat{W}^2(kR)\, \mathrm{d}\ln k, \tag{5}$$

and the correlation function is, in addition, modulated by the zeroth order spherical Bessel function $j_0(x) = \sin(x)/x$,

$$\xi_R(r) = \int_0^\infty \Delta^2(k) \hat{W}^2(kR) j_0(kr)\, \mathrm{d}\ln k. \tag{6}$$

The explicit expression of $\hat{W}(kR)$ is

$$\hat{W}(kR) = \frac{3}{kR} j_1(kR) = 3\frac{\sin(kR) - kR\cos(kR)}{(kR)^3}. \tag{7}$$

Unfortunately, in practice, we are not able to directly access the matter power spectrum. The reason is that the galaxies we observe do not directly probe the distribution of matter in the universe. In fact, they represent a discrete biased sampling of the underlying matter density field and the biasing function is, a priori, not known. A way to overcome this problem is to refine the independent measurements of the bias function through weak lensing surveys. Otherwise, one can parametrize the bias adding additional nuisance parameters to the model and, consequently, marginalize over them.

A completely different approach, however, is to seek new statistical observables, which can be considered to be unbiased by construction. This is the path followed by Bel & Marinoni (2014) by introducing the clustering ratio,

$$\eta_R(r) \equiv \frac{\xi_R(r)}{\sigma_R^2}, \tag{8}$$

that is the ratio of the correlation function over the variance of the smoothed field.

We assume that the relation between the matter density contrast and the galaxy (or halo) density field is a local and deterministic mapping, which is regular enough to allow a Taylor expansion (Fry & Gaztanaga 1993) as

$$\delta_{g,R} = F(\delta_R) \simeq \sum_{i=1}^{N} \frac{b_i}{i!}\delta_R^i. \tag{9}$$

Moreover we assume the growth of fluctuations to occur hierarchically (see Bernardeau et al. 2002; Bel & Marinoni 2012), so that each higher order cumulant moment can be expressed according to powers of the variance and two-point correlation function,

$$\begin{aligned} \langle \delta_R^n \rangle_c &= S_n \sigma_R^{2(n-1)}, \\ \langle \delta_{i,R}^n \delta_{j,R}^m \rangle_c &= C_{nm} \xi_R(r) \sigma_R^{2(n+m-2)}, \end{aligned} \tag{10}$$

the former applying to the one-point statistics and the latter to the two-point ones.

It has been shown by Bel & Marinoni (2012) that the bias function only modifies the clustering ratio of galaxies at the next order beyond the leading one and that it is not sensitive to third-order bias

$$\begin{aligned} \eta_{g,R}(r) \simeq\ & \eta_R(r) + \frac{1}{2} c_2^2 \eta_R(r) \xi_R(r) \\ & - \left\{ (S_{3,R} - C_{12,R}) c_2 + \frac{1}{2} c_2^2 \right\} \xi_R(r), \end{aligned} \tag{11}$$

where $c_2 \equiv b_2/b_1$. By choosing a sufficiently large smoothing scale, the higher order contribution in equation (11) becomes negligible and we obtain

$$\eta_{g,R}(r) = \eta_R(r), \tag{12}$$

meaning that in this case the clustering ratio of galaxies can be directly compared to the clustering ratio predicted for the matter distribution.

The local biasing model is not the best way of describing the bias function between matter and haloes/galaxies (Mo & White 1996; Sheth & Lemson 1999; Somerville et al. 2001; Casas-Miranda et al. 2002). It can be improved by introducing a non-local component depending on the tidal field. However, it has been shown by Chan, Scoccimarro & Sheth (2012) and by Bel, Hoffmann & Gaztañaga (2015) that, when dealing with statistical quantities which are averaged over all possible orientations, then the non-local component is degenerate with the second order bias c_2, thus expression (11) remains valid and we do not consider non-local bias in our analysis.

On linear scales, the clustering ratio is expected to be independent from redshift. Since, in a ΛCDM universe, we can write [normalizing all quantities to the present time variance on the scale $r_8 = 8\,h^{-1}$ Mpc, $\sigma_8^2(z=0)$] the evolution of the variance and the correlation function as

$$\begin{aligned} \sigma_R^2(z) &= \sigma_8^2(z=0) D^2(z) \mathcal{F}_R \\ \xi_R(r,z) &= \sigma_8^2(z=0) D^2(z) \mathcal{G}_R(r), \end{aligned} \tag{13}$$

where $D(z)$ is the linear growth factor of matter density fluctuations and

$$\begin{aligned} \mathcal{F}_R &= \frac{\int_0^\infty \Delta^2(k) \hat{W}^2(kR)\,\mathrm{d}\ln k}{\int_0^\infty \Delta^2(k) \hat{W}^2(kr_8)\,\mathrm{d}\ln k} \\ \mathcal{G}_R(r) &= \frac{\int_0^\infty \Delta^2(k) \hat{W}^2(kR) j_0(kr)\,\mathrm{d}\ln k}{\int_0^\infty \Delta^2(k) \hat{W}^2(kr_8)\,\mathrm{d}\ln k}, \end{aligned}$$

depend only on the shape of the power spectrum. Hence, the clustering ratio $\xi_R(r)/\sigma_R^2 = \mathcal{G}_R(r)/\mathcal{F}_R$, does not depend on $D(z)$, which cancels outs.

In practice, we include weak non-linearities which introduce a small, but nevertheless detectable, redshift dependence.

Measurements of the clustering of galaxies are not only biased with respect to predictions for the matter field, but they also are affected by the peculiar motion of galaxies. This motion introduces a spurious velocity component (along the line of sight) that distorts the redshift assigned to galaxies. Since, for the clustering ratio, we are interested in large smoothing scales and separations, we can focus on the linear scales, where the only effect is due to the coherent motion of infall of galaxies towards the overdense regions in the universe.

We can link the position of a galaxy (or dark matter halo) in real space to its apparent position in redshift-space. Let us denote $\boldsymbol{r}$ as the true comoving distance along the line of sight; in redshift space it becomes

$$\boldsymbol{s} = \boldsymbol{r} + \frac{v_{\mathrm{p}\parallel}\,(1+z)}{H(z)} \hat{\boldsymbol{e}}_r, \tag{14}$$

where $v_{\mathrm{p}\parallel}$ is the line-of-sight component of the peculiar velocity and $\hat{\boldsymbol{e}}_\mathbf{r}$ is the line-of-sight versor. Considering the Fourier space decomposition of the density contrast, the relation linking its value in redshift space to the one in real space (Kaiser 1987) is

$$\delta^s(\boldsymbol{k}) = (1 + f\mu^2)\delta(\boldsymbol{k}), \tag{15}$$

where quantities in redshift space are expressed with the superscript s and μ is the cosine of the angle between the wavemode $\boldsymbol{k}$ and the line of sight. Here f is the so called growth rate, defined as the logarithmic derivative of the growth factor of structures with respect to the scale factor, $f \equiv \mathrm{d}\ln D/\mathrm{d}\ln a$. Averaging over all angles ϑ, the variance and the correlation function in redshift space result modified by the same multiplicative factor

$$\begin{aligned} {\sigma_R^s}^2 &= K\sigma_R^2 \\ \xi_R^s(r) &= K\xi_R(r) \end{aligned} \tag{16}$$

where $K = 1 + 2f/3 + f^2/5$ is the Kaiser factor. As a consequence, the clustering ratio is unaffected by redshift-space distortions on linear scales. This argument allows us to rewrite the identity (12) as

$$\eta_{g,R}^s(r) \equiv \eta_R(r), \tag{17}$$

meaning that, by properly choosing the smoothing scale R and the correlation length r, measurements of the clustering ratio from galaxies in redshift space can be directly compared to predictions for the clustering ratio of matter in real space.

2.1 Estimators

The clustering ratio can be estimated from count-in-cells, where, under the assumption of ergodicity, all ensemble averages become spatial averages. We follow the counting process set up by Bel & Marinoni (2012), we define the discrete density contrast as

$$\delta_{N,i} = \frac{N_i}{\bar{N}} - 1, \tag{18}$$

where N_i is the number of objects in the i-th cell and $\bar{N}$ is the mean number of objects per cell. The estimator of the variance is therefore

$$\hat{\sigma}_R^2 = \frac{1}{p}\sum_{i=1}^{p} \delta_i^2 \tag{19}$$

and the one of the correlation function is

$$\hat{\xi}_R(r) = \frac{1}{pq}\sum_{i=1}^{p}\sum_{j=1}^{q}\delta_i\delta_j \tag{20}$$

leading to the definition of the estimator of the clustering ratio as

$$\hat{\eta}_R(r) = \frac{\hat{\xi}_R(r)}{\hat{\sigma}^2_R}. \tag{21}$$

Throughout this work we will often express the correlation length r as a multiple of the smoothing scale, i.e. $r = nR$.

Since we are dealing with a discrete counting process, the shot noise needs to be properly accounted for. We follow the approach of Bel & Marinoni (2012) and correct the estimator of the variance according to

$$\hat{\sigma}^2_R = \langle \delta^2_n(\boldsymbol{x})\rangle - \frac{1}{\bar{N}} = \frac{1}{p}\sum_{i=1}^{p}\delta_i^2 - \frac{1}{\bar{N}}, \tag{22}$$

where $\bar{N}$ is the mean number of objects per cell. On the other hand, the correlation function needs no correction, as long as the spheres do not overlap.

2.2 Effects of massive neutrinos

We introduce massive neutrinos as a subdominant dark matter component. For simplicity, we consider three degenerate massive neutrinos, with total mass $M_\nu = \sum_i m_{\nu,i}$ and present-day neutrino energy density in units of the critical density of the universe $\Omega_{\nu,0}h^2 = M_\nu/(93.14\,\mathrm{eV})$. The neutrino fraction is usually expressed with respect to the total matter as $f_\nu = \Omega_\nu/\Omega_\mathrm{m}$. For a more complete treatment of neutrinos in cosmology, we refer the reader to Lesgourgues & Pastor (2006, 2012, 2014).

Neutrinos of sub-eV mass, which seem to be the most likely candidates both from particle physics experiments and cosmology, decouple from the primeval plasma when the weak interaction rate drops below the expansion rate of the universe, at a time when the background temperature is around $T \simeq 1$ MeV. This corresponds to a redshift $1 + z_\mathrm{dec} \sim 10^9$. Since the redshift of their non-relativistic transition, obtained equating their rest-mass energy and their thermal energy, is given by

$$1 + z_{nr} \simeq 1890\,\frac{m_{\nu,i}}{1\ \mathrm{eV}}, \tag{23}$$

when neutrinos decouple, they are still relativistic. As a consequence, since the momentum distribution of any species is frozen at the time of decoupling, neutrino momenta keep following a Fermi–Dirac distribution even after their non-relativistic transition, and neutrinos end up being characterized by a large velocity dispersion. An effective description of the evolution of neutrinos can be achieved employing a fluid approximation (Shoji & Komatsu 2010). In this framework we can define a neutrino pressure, $p_\nu = w_\nu\rho_\nu c^2$, computed integrating the momentum distribution. Such pressure is characterized by an effective adiabatic speed of sound (Blas et al. 2014)

$$c_{s,i} = 134.423\,(1+z)\,\frac{1\ \mathrm{eV}}{m_{\nu,i}}\ \mathrm{km\,s^{-1}}, \tag{24}$$

that represents the speed of propagation of neutrino density perturbations. Such speed of sound defines the minimum scale under which neutrino perturbations cannot grow, called the free streaming scale. It corresponds to a wavenumber

$$k_\mathrm{FS}(z) = \left[\frac{4\pi G\bar{\rho}a^2}{c_s^2}\right]^{1/2} = \left[\frac{3}{2}\frac{H^2\Omega_\mathrm{m}(z)}{(1+z)^2c_s^2}\right]^{1/2}, \tag{25}$$

or a proper wavelength

$$\lambda_\mathrm{FS} = 2\pi a/k_\mathrm{FS}. \tag{26}$$

At each redshift, neutrino density fluctuations of wavelength smaller than the free streaming scale are suppressed, their gravitational collapse being contrasted by the fluid pressure support. As a consequence, neutrinos do not cluster on small scales and remain more diffuse compared to the cold matter component.

Neutrino free streaming does not only affect the evolution of neutrino perturbations, in fact it affects the evolution of all matter density fluctuations. We can model the growth of matter fluctuations employing a two-fluid approach (Blas et al. 2014; Zennaro et al. 2017). In this case, the solution of the equations of growth for the neutrino and cold matter fluids are coupled,

$$\begin{cases} \ddot{\delta}_\mathrm{cb} + \mathcal{H}\dot{\delta}_\mathrm{cb} - \frac{3}{2}\mathcal{H}^2\Omega_\mathrm{m}\left\{f_\nu\delta_\nu + (1-f_\nu)\delta_\mathrm{cb}\right\} = 0 \\ \ddot{\delta}_\nu + \mathcal{H}\dot{\delta}_\nu - \frac{3}{2}\mathcal{H}^2\Omega_\mathrm{m}\left\{\left[f_\nu - \frac{k^2}{k^2_\mathrm{FS}}\right]\delta_\nu + (1-f_\nu)\delta_\mathrm{cb}\right\} = 0, \end{cases} \tag{27}$$

where derivatives are taken with respect to conformal time, $\mathrm{d}\tau = \mathrm{d}t/a$, and both the Hubble function and the matter density parameter are functions of time, $\mathcal{H} = \mathcal{H}(\tau)$ and $\Omega_\mathrm{m} = \Omega_\mathrm{m}(\tau)$.

The coupling of these equations requires the evolution of the CDM density contrast to be scale dependent, unlike in standard ΛCDM cosmologies. We therefore expect to find an observable suppression even in the CDM+baryon power spectrum, starting from the mode corresponding to the size of the free-streaming scale at the time of the neutrino non-relativistic transition, $k_\mathrm{nr} = k_\mathrm{FS}(z_\mathrm{nr})$, and affecting all the scales smaller than this one.

3 CLUSTERING RATIO WITH MASSIVE NEUTRINOS

In order to investigate the behaviour of the clustering ratio in cosmologies with massive neutrinos, i.e. whether it maintains all the properties described in Section 2, we analyse the cosmological simulations DEMNUni, presented in Castorina et al. (2015) and Carbone, Petkova & Dolag (2016).

These simulations have been performed using the GADGET-III code by Viel, Haehnelt & Springel (2010) based on the GADGET simulation suite (Springel et al. 2001; Springel 2005). This version includes three active neutrinos as an additional particle species.[1]

The DEMNUni project comprises two set of simulations. The first one, which is the one considered in this work, includes four simulations, each implementing a different neutrino mass. Besides the reference ΛCDM simulation, which has $M_\nu = 0$ eV, the other ones are characterized by $M_\nu = \{0.17, 0.30, 0.53\}$ eV. The second set includes 10 simulations, exploring different combinations of neutrino masses and dynamical dark energy parameters.

All simulations share the same *Planck*-like cosmology, with Hubble parameter $H_0 = 67\,\mathrm{km\,s^{-1}\,Mpc^{-1}}$, baryon density parameter

[1] The simulations do not account for an effective neutrino number $N_\mathrm{eff} > 3$, as possible neutrino isocurvature perturbations which could produce larger N_eff (therefore affecting galaxy and CMB statistics Carbone, Mangilli & Verde 2011a) are currently excluded by present data (see e.g. Di Valentino & Melchiorri 2014).

Table 1. The cosmological parameters that vary among the four DEMNUni simulations considered in this work, depending on the assumed neutrino total mass.

	ΛCDM	NU0.17	NU0.30	NU0.53
M_ν (eV)	0	0.17	0.30	0.53
Ω_c	0.27	0.2659	0.2628	0.2573
$\sigma_{8,\,cc}$	0.846	0.813	0.786	0.740

$\Omega_b = 0.05$, primordial spectral index $n_s = 0.96$, primordial amplitude of scalar perturbations $A_s = 2.1265 \times 10^9$ (at a pivotal scale $k_p = 0.05\,\mathrm{Mpc}^{-1}$) and optical depth at the time of recombination $\tau = 0.0925$. The density parameter of the cold dark matter, Ω_{cdm}, is adjusted in each simulation, depending on the neutrino mass, so that all simulations share the same total matter density parameter $\Omega_m = 0.32$, see Table 1. Each simulation follows the evolution of 2048^3 CDM particles and, when present, 2048^3 neutrino particles, in a comoving cube of $2\,h^{-1}$ Gpc side. The mass of the CDM particle is $\sim 8 \times 10^{10}\,h^{-1}\,\mathrm{M}_\odot$, and changes slightly depending on the value of Ω_{cdm}. All simulations start at an initial redshift $z_{in} = 99$ and reach $z = 0$ with 62 comoving outputs at different redshifts. In this work we focus on the snapshots at redshift $z = 0.485\,51$ and $z = 1.053\,52$.

Dark matter haloes have been identified through a Friend-of-Friends (FoF) algorithm with linking length $b = 0.2$ and setting the minimum number of particles needed to form a halo to 32. Thus, the least massive haloes have mass of about $2.6 \times 10^{12}\,h^{-1}\,\mathrm{M}_\odot$. In order to check the stability of our results regarding the choice of the definition of a halo, we also have access to halo catalogues where haloes have been identified using spherical overdensities. For the purpose of this work we constructed halo catalogues in redshift space by modifying the positions along the z direction according to the projected velocity (properly converted in length) in that direction (see equation 14).

Regarding error estimation, as they are very large simulations, a jackknife method has been implemented by subdividing the box in 64 sub-cubes. The standard error on the measured value of $\eta_R(r)$ is then taken to be the dispersion obtained from the jackknife process

$$\sigma^2_{\eta_R} = \frac{N_j - 1}{N_j} \sum_{i=1}^{N_j} \left[\eta_{R,i}(r) - \bar{\eta}_R(r)\right]^2, \tag{28}$$

where N_j is the number of jackknife resamplings, in our case $N_j = 64$.

In the following, we first check the reliability of the clustering ratio in the presence of massive neutrinos. In particular we are interested in proving that the identity $\eta^z_{R,g}(r) \equiv \eta_R(r)$ still holds. To this end, we must prove that the clustering ratio at the scales of interest does not depend on the galaxy–matter bias (so that we can compare predictions for matter and measurements from galaxies) and that it is not affected by redshift-space distortions (to be safe when comparing the real space predictions to measurements obtained in a galaxy redshift survey).

3.1 Bias sensitivity

In order to test the independence of the clustering ratio from the bias on linear scales, we divide the dark matter haloes in nine mass bins, reported in Table 2. The various halo populations evolve in a different way, therefore they present different biasing functions with respect to the dark matter field. Thus, we will use the linear bias b_L to characterize each halo sample. In Table 3 we show how both the FoFs and the spherical overdensities from the simulations populate these mass bins in the simulations. Due to the minimum number of particle required to identify a halo, the first two mass bins do not contain any. On the other hand, the only mass limit to the spherical overdensities is given by the mass resolution of the simulation, hence all the mass bins are populated.

Table 2. Subdivision of the halo catalogues in mass bins.

Bin	Mass range ($10^{12}\,h^{-1}\,\mathrm{M}_\odot$)
0	$0.58 \le M < 1.16$
1	$1.16 \le M < 2.32$
2	$2.32 \le M < 3.28$
3	$3.28 \le M < 4.64$
4	$4.64 \le M < 6.55$
5	$6.55 \le M < 9.26$
6	$9.26 \le M < 30$
7	$30 \le M < 100$
8	$M \ge 100$

In Fig. 1 we show the estimated correlation functions of each FoF sample in the two extreme cases of $M_\nu = 0$ eV and $M_\nu = 0.53$ eV (the same holds for the SOs as well).

We also represent the corresponding correlation function of the cold matter field, which is used to estimate the linear bias b_L characterizing each halo sample:

$$b_L \equiv \sqrt{\frac{\xi^{FoF}_R(nR)}{\xi_R(nR)}}. \tag{29}$$

We find that our cut in mass does indeed correspond to different tracers, with higher bias for higher mass objects. However, such different halo populations still show a constant bias with respect to scale, which allows us to fit the measured bias in Fig. 1 with flat lines.

The independence of the FoF-matter bias from scale is confirmed also in the massive neutrino case (Fig. 1, right). In particular, we note here that the bias is generally higher when considering massive neutrinos. This is due to the fact that, since they smooth the matter distribution, neutrinos make haloes of a given mass rarer then in a standard ΛCDM cosmology.

Secondly we compute the clustering ratio for both the FoFs and the spherical overdensities at redshift $z = 0.485\,51$ and $z = 1.053\,52$. In each of these cases, we analyse the ΛCDM simulation, which does not include massive neutrinos, and the ΛCDMν simulations with $M_\nu = \{0.17, 0.30, 0.53\}$ eV. In the two plots in Fig. 2 we show the clustering ratio for fixed smoothing radius $R = 16\,h^{-1}$ Mpc and correlation length $r = 2R$ in the same mass bins shown in Table 2 for the FoFs and spherical overdensities respectively. Points are measurements in the simulations, while lines are the predictions obtained from the cold matter power spectrum. The ratio between measurements and predictions is in the bottom panel.

At $z = 0.485\,51$, the measured clustering ratio in the bins with masses $<30.43 \times 10^{12}\,h^{-1}\,\mathrm{M}_\odot$ agrees with the predictions for the matter at 3 per cent level. Below $100\,h^{-1}\,\mathrm{M}_\odot$ the agreement is within 5 per cent. For objects with mass greater than this, we observe a more scattered trend. We blame a lower statistical robustness, due to fewer objects falling in these mass bins. In any case, we do not observe any peculiar dependence of the clustering ratio on the mass of the objects, confirming up to a few per cent accuracy its independence on the bias at these scales.

At $z = 1.053\,52$, for low-mass haloes ($<10^{12}\,h^{-1}\,\mathrm{M}_\odot$) the measurements are still compatible with a deviation lower than 3 per cent.

Table 3. Population of the nine mass bins for the FoF and spherical overdensities with respect to the critical density (SO) at redshift $z = 0.485\,51$ and $z = 1.053\,52$.

			bin 0	bin 1	bin 2	bin 3	bin 4	bin 5	bin 6	bin 7	bin 8
FoF	$z = 0.485\,51$	$M_\nu = 0.00$ eV	0	0	2902 221	3509 393	2402 274	1708 375	2878 557	758 008	145 410
		$M_\nu = 0.17$ eV	0	0	3152 025	3178 910	2430 866	1667 315	2712 374	690 356	122 241
		$M_\nu = 0.30$ eV	0	0	3116 471	3269 324	2263 001	1642 694	2589 654	634 844	104 539
		$M_\nu = 0.53$ eV	0	0	3273 517	3026 718	2144 285	1501 769	2334 332	532 432	76 127
	$z = 1.053\,52$	$M_\nu = 0.00$ eV	0	0	2571 902	3039 264	2003 119	1358 767	2044 706	389 064	38 299
		$M_\nu = 0.17$ eV	0	0	2713 196	2674 546	1958 721	1277 479	1836 860	328 973	28 852
		$M_\nu = 0.30$ eV	0	0	2620 295	2674 912	1767 015	1218 810	1679 768	283 298	22 244
		$M_\nu = 0.53$ eV	0	0	2619 539	2335 248	1570 202	1036 782	1386 909	206 588	13 059
SO	$z = 0.485\,51$	$M_\nu = 0.00$ eV	453 415	2973 241	2783 664	2361 431	1669 494	1210 036	2064 503	527 389	88 178
		$M_\nu = 0.17$ eV	471 602	2993 986	2904 400	2118 437	1668 026	1166 042	1917 029	470 522	72 097
		$M_\nu = 0.30$ eV	486 007	2997 527	2842 491	2159 522	1559 049	1112 575	1806 821	424 202	60 046
		$M_\nu = 0.53$ eV	508 713	3259 563	2582 711	1956 593	1424 500	1014 066	1587 591	343 288	41 497
	$z = 1.053\,52$	$M_\nu = 0.00$ eV	363 148	2449 897	2433 901	2030 689	1373 779	952 365	1446 087	263 959	22 482
		$M_\nu = 0.17$ eV	359 806	2376 103	2479 355	1766 898	1330 746	885 172	1280 841	218 832	16 462
		$M_\nu = 0.30$ eV	354 938	2304 946	2374 992	1750 620	1206 312	819 053	1157 522	184 575	12 287
		$M_\nu = 0.53$ eV	341 645	2359 735	2069 025	1500 656	1039 892	694 588	932 357	130 319	6 834

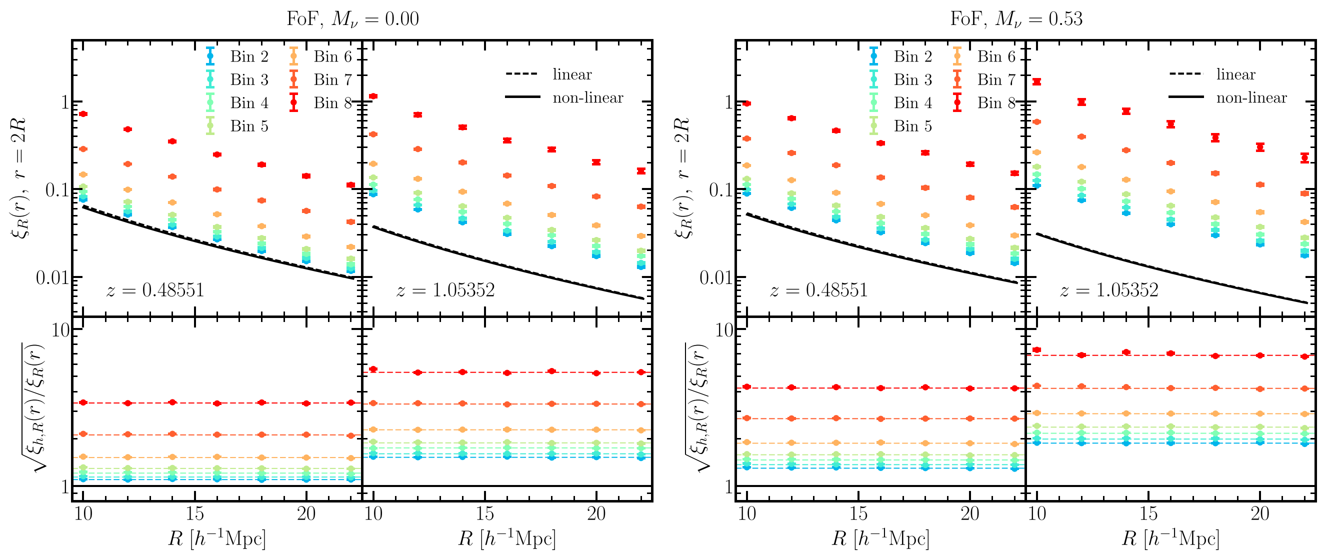

Figure 1. Correlation function of haloes identified in the simulation via the FoF halo-finder, in two different cosmologies. The left and right plots show measurements in the ΛCDM and ΛCDMν (with $M_\nu = 0.53$ eV) cosmologies, respectively. In both cases, the left-hand panel is at redshift $z = 0.485\,51$ and the right one at $z = 1.05352$. In the top panel we show the correlation function measured in the mass bins presented in Table 2 (points) compared to the theoretical smoothed cold matter correlation function (black solid line). The bottom panel shows the halo-matter bias for the FoF case, computed as $b = \sqrt{\xi_R^{\rm FoF}(r)/\xi_R(r)}$. The linear bias in the simulation with massive neutrinos is larger than in the standard ΛCDM case, because, as neutrinos suppress structure clustering, massive haloes become rarer. We fit the bias values with a straight line between $R = 16$ and $22\,h^{-1}$Mpc. As the fit shows, the linear bias is compatible with the scale-independent theoretical prediction.

However, the high-mass bins exhibit a stronger and systematic dependence (with respect to the $z \sim 0.5$ case), which seems to depend on the neutrino mass. Despite the fact that in this large-mass regime halo clustering might suffer from exclusion effects (Manera & Gaztañaga 2011), leading to sub-Poisson shot noise, the observed trend can be qualitatively predicted. Since the halo–halo two-point correlation of regions which will eventually form haloes can be predicted (assuming spherical collapse) in the initial configuration of the density field, and given that the mass function is known, we can derive the mass-dependence of the biasing coefficients and predict the halo two-point correlation function at a given redshift (see Desjacques, Jeong & Schmidt 2016, for a detailed review). Within this framework we obtain a prediction of the mass dependence of the clustering ratio that qualitatively matches the trend observed in Fig. 2. We use this as a diagnostic to make sure that we are well within the mass range in which the clustering ratio is accurately predicted. We conclude that this effect becomes worrisome only for tracers with $M > 3 \times 10^{13}\,h^{-1}\,\mathrm{M}_\odot$ at redshift $z \sim 1$ (corresponding to tracers with linear bias around 3), while we are ultimately interested in galaxies, whose masses and typical Lagrangian sizes are by far smaller and whose redshift is mainly around $z \sim 0.5$. As a consequence, we can safely neglect this effect in the rest of our present analysis.

As confirmed by Fig. 2 we find similar results for both the FoFs and the SO, and therefore such results do not depend on the tracer we choose to observe.

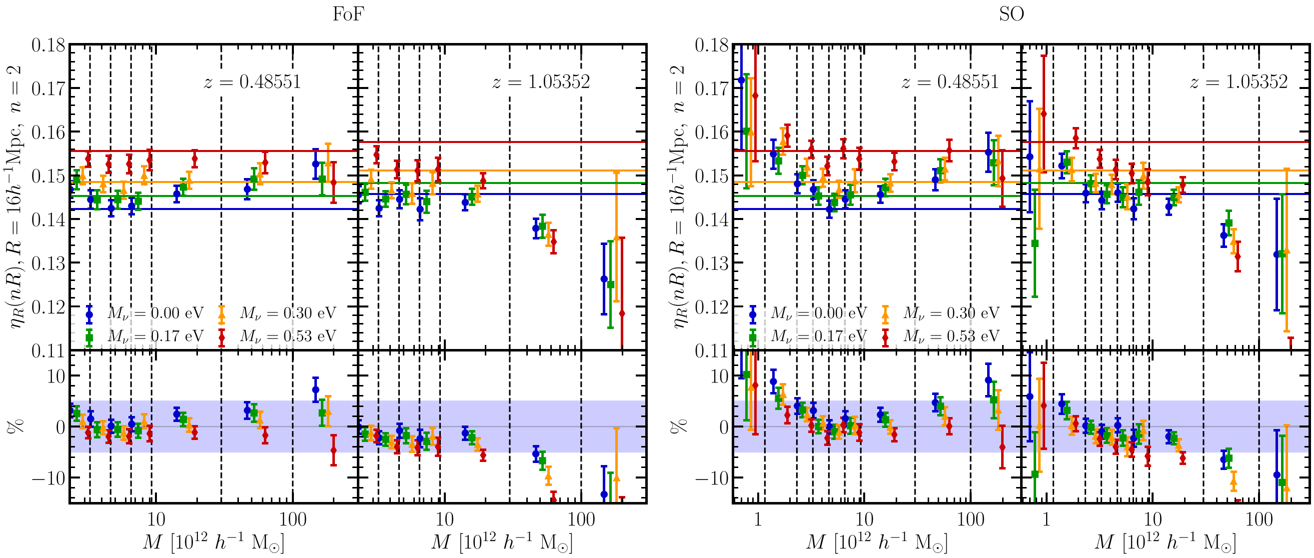

Figure 2. Dependence of the clustering ratio on the mass of haloes identified via FoF (left-hand panel) and spherical overdensity (SO, right-hand panel) at redshift $z = 0.485\,51$ and $z = 1.053\,52$ for all the neutrino masses. The smoothing radius is $R = 16\,h^{-1}$ Mpc and the correlation length is twice the smoothing radius. Symbols with error bars show measurements in the simulations, while solid lines represent the theoretical expectation for the cold matter. In the bottom panel we show the relative difference between the measurements and theoretical predictions, the shaded area represents a -5, $+5$ per cent deviation.

Finally, we claim that the clustering ratio is insensitive to the bias on linear scales in a cosmology including massive neutrinos irrespective of either the mass of the tracer or the nature of the tracer itself or the total mass of neutrinos considered. This allows us to directly compare real-space predictions of the matter clustering ratio with real-space measurements of the clustering ratio of any biased matter tracer, i.e. $\eta_{g,\,R}(r) \equiv \eta_R(r)$.

3.2 Redshift space

In redshift space, as described in Section 2, the apparent position of galaxies is modified according to the projection of their peculiar velocity along the line of sight. This effect distorts the clustering properties of the distribution and we thus expect its correlation function and variance to be affected. However, we do not expect redshift-space distortions to affect the clustering ratio on linear scales (equation 17) as the effect cancels out into the ratio. In order to verify the accuracy of this approximation we created the redshift space catalogues of the FoFs and spherical overdensities in the simulations, moving the positions of the tracers along an arbitrary direction, chosen as the line-of-sight direction.

Having shown that the clustering ratio does not depend on the way we define the haloes nor on their mass tracer, from now on we focus on the dark matter halo catalogues identified with the FoF algorithm and we compare the two extreme cases of $M_\nu = 0$ eV and $M_\nu = 0.53$ eV. Note that we use the $M_\nu = 0$ simulation as a reference for comparisons, since it has already been shown that these properties are valid when neutrino are massless (see Bel & Marinoni 2014; Bel et al. 2014).

Fig. 3 shows, at the scales of interest, the independence of the clustering ratio from redshift-space distortions. The ratio between measurements of the clustering ratio in redshift and in real space is of order 1, either with and without massive neutrino, both at $z = 0.485\,51$ and $z = 1.053\,52$.

In particular we show that we recover the results already obtained in other works (Bel & Marinoni 2012) in the ΛCDM case. In the case including massive neutrinos we find an agreement between

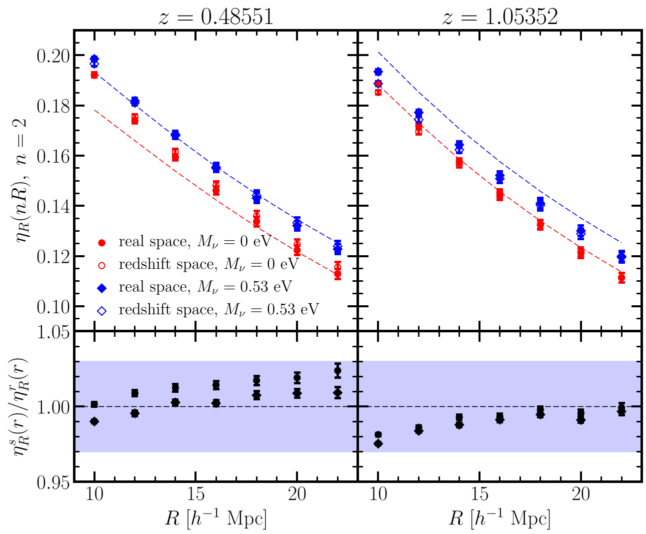

Figure 3. The clustering ratio smoothed on the scale R and at correlation length $r = nR, n = 2$ as a function of the smoothing scale. We show in red the measurements in the ΛCDM simulation and in blue the ones in the simulation with the highest neutrino mass, $M_\nu = 0.53$ eV, which represent the two extreme cases for the neutrino mass considered in this work. Filled dots are measurements in real space, while empty dots represent redshift space measurements. In the bottom panel the ratio between the clustering ratio in redshift space over the real space case is shown. Since on linear scales the monopole contribution coming from redshift-space distortions enhances the correlation function and the variance by the same multiplicative factor, we expect the clustering ratio to be unaffected. The ratio between redshift and real space measurements is, in fact, of order 1 with an accuracy better than 3 per cent. This trend is confirmed from measurements at redshift $z = 1.053\,52$ (right), being the matter growth more linear at higher redshifts.

redshift and real space measurements at 3 per cent level at redshift $z = 0.485\,51$ and at better than 1 per cent on scales $R \gtrsim 16\,h^{-1}$ Mpc at $z = 1.053\,52$. In this case the accuracy is higher at higher redshift as the growth of structures is more linear.

Moreover we note that the agreement with predictions is better for the simulation with massive neutrinos with respect to the ΛCDM one. This is due to the fact that massive neutrinos lower the matter fluctuations (see the values of $\sigma_{8,\,\mathrm{cc}}$ in Table 1) and therefore tend to reduce the velocity dispersion, resulting in redshift-space distortions that are more into the linear regime.

We therefore propose to use the clustering ratio as a cosmological probe to constrain the parameters of the cosmological model. As a matter of fact, the analysis of the simulations has shown that the clustering ratio, besides being independent from the matter tracer and the bias, is not affected by redshift-space distortions on linear scales. This implies that equation (17), $\eta^{s}_{g,R}(r) \equiv \eta_R$, still holds in the presence of massive neutrinos, allowing us to directly compare clustering ratio measurements in redshift-survey galaxy catalogues to the theoretical matter clustering ratio predictions.

4 RESULTS

4.1 Optimization

In order to estimate and predict the clustering ratio of galaxies, we need to choose two different scales: the smoothing scale R, i.e. the radius of the spheres we use for counting objects, and the correlation length r, that for simplicity we assume to be some multiple of the smoothing scale, $r = nR$. Choosing the best combinations of R and r is vital to maximize the information we can extract from this statistical tool.

The smoothing scale R controls the scale under which we make our observable blind to perturbations. A sufficiently large value of R allows us to screen undesired non-linear effects, that would compromise the effectiveness of the clustering ratio. On the other hand, an excessively large smoothing scale can lead to more noisy measurements, since in the same volume we can accommodate fewer spheres. Moreover, if R is too large, the entire signal would be screened and the measurement would become of little interest.

Also for the correlation length, choosing small values of R and n implies coping with small-scale non-linearities, which risk to invalidate the identity expressed in equation (17). Large values of correlation distances, however, would make it difficult to accommodate enough couples of spheres in the volume to guarantee statistical robustness. An additional constraint comes from the strategy we adopt to fill the volume with spheres and perform the count-in-cells. In this framework, if the correlation length is below twice the smoothing scales, $r < 2R$, the spheres of our motif of cells would overlap, resulting in an additional shot-noise contribution. For this reason, we only allow values of $n \geq 2$.

The main information we want to extract is the total neutrino mass. The sensitivity of the clustering ratio to this parameter can be quantified as an effective signal-to-noise ratio, defined as

$$\mathrm{S/N} = \frac{\eta^{\nu}_R(r) - \eta^{\Lambda}_R(r)}{\sigma^{\Lambda}_R}, \tag{30}$$

where $\eta^{\nu}_R(r)$ is the clustering ratio measured in a simulation with neutrino mass M_ν, $\eta^{\Lambda}_R(r)$ is measured in the reference ΛCDM simulation and σ^{Λ}_R is the uncertainty on the clustering ratio measured in the ΛCDM simulation. This quantity estimates how much a massive neutrino cosmology is distinguishable from a ΛCDM one, given the typical errors on the measurements of the clustering ratio for the specific volume and number density of tracers, as a function of R and r. Fig. 4 shows the (n, R) plane, constructed as a grid with correlation lengths $n \in [2, 2.75]$ with step $\Delta n = 0.05$ and smoothing scales $R \in [15, 30]$ with step $\Delta R = 1$, all distances being expressed in units of h^{-1} Mpc. At each point on the grid a colour is associated, representing the value of this effective signal-to-noise ratio. The effect of massive neutrinos is, as expected, appreciable on small scales (both small n and small R), and eventually becomes negligible moving towards large scales. While we want to maximize the effects of neutrinos, we want to minimize errors. In particular, we can define a theoretical error, that accounts for the combinations of smoothing radii R and correlation lengths r where the assumptions under which we can apply the identity expressed in equation (17) break down. Such theoretical error can be quantified as

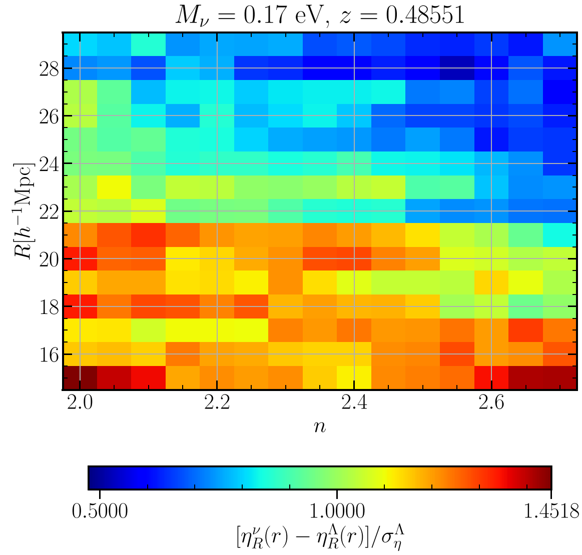

Figure 4. The effect of neutrinos on the clustering ratio compared to a ΛCDM cosmology. In the (n, R) plane, we plot colour contours corresponding to $(\eta_R(r, \nu) - \eta_R(r, \Lambda\mathrm{CDM})/\sigma_\eta(\Lambda\mathrm{CDM})$. As expected, the sensitivity to the neutrino total mass increases at small smoothing scales and correlation lengths (red regions).

$$\delta_{\mathrm{th}} = \frac{\eta_R(r) - \eta^{\mathrm{th}}_R(r)}{\sigma_\eta}, \tag{31}$$

where $\eta_R(r)$ is the clustering ratio measured in the simulation with a given cosmology, $\eta^{\mathrm{th}}_R(r)$ is the prediction obtained with a Boltzmann code, and σ_η the uncertainty on the measurements. In Fig. 5 we show as a colour map the values that we obtain for this theoretical error in the same (n, R) plan introduced above. We can see that on very small scales the effect of non-linearities is not negligible, and we cannot use the clustering ratio as an unbiased observable.

From Figs 4 and 5 we see that we need to balance between the requirement coming from the signal-to-noise ratio (that is maximum on small scales), and those from the theoretical errors (that is minimum on large scales). We introduce, therefore, a way of combining these pieces of information into a single colour map, which we use to seek the sweet-spots, in this parameter space, where both conditions are satisfied.

First, we define a combined percentage error (that accounts both for statistical errors and discrepancies from the model) as

$$\delta_{\mathrm{combined}} = \left\{ \frac{\eta^{\nu}_R(r) - \eta^{\nu,\mathrm{th}}_R(r)}{\eta^{\nu}_R(r) - \eta^{\Lambda}_R(r)} \right\} \left\{ \frac{\sigma^{\Lambda}_\eta}{\eta^{\nu}_R(r) - \eta^{\Lambda}_R(r)} \right\}. \tag{32}$$

The quantity in the first parenthesis is related to how much the statistical error is important with respect to the effects of neutrinos, while the second parenthesis is a weight that accounts for the typical uncertainty on the measurement in each bin of n and R. Finally, we

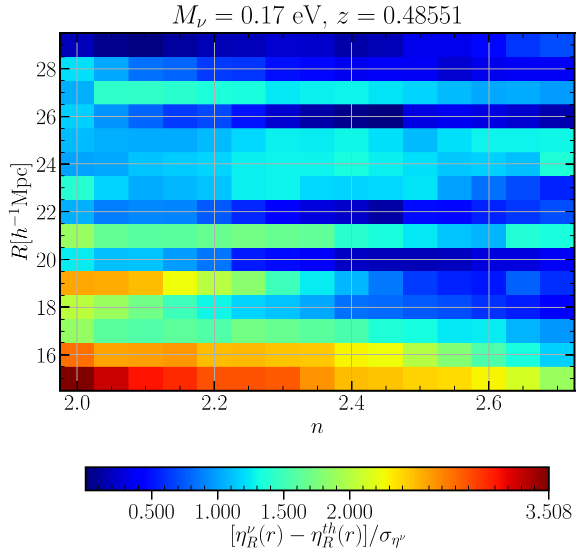

Figure 5. Discrepancy between the clustering ratio measured in the simulation and the theoretical prediction in the (n, R) plane. Colours represent the quantity $(\eta_R(r) - \eta_R^{\rm th}(r))/\sigma_R^{(r)}$, the blue regions being the ones with the best agreement with the predictions. Sufficiently large smoothing scales screen the effects of the non-linear growth of perturbations, allowing us to exploit the clustering ratio as a cosmological probe. By smoothing our distribution on scales $R > 19\,h^{-1}$ Mpc, we ensure an agreement with the model better then ∼1.5 standard deviations.

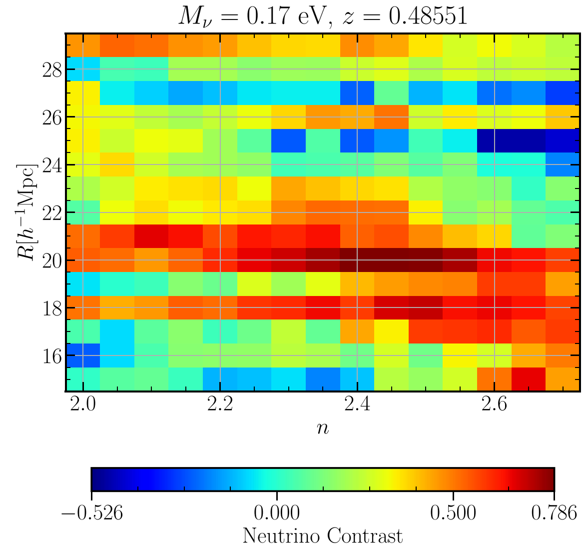

Figure 6. In this colour plot we subtract to the neutrino signal-to-noise normalized to 1 a combined error normalized in the same fashion. Details on the definition are in the text. We are interested to regions in the (n, R) plane where the neutrino signal-to-noise dominates (∼1) on the error (∼0), graphically visible as hot spots. The region with smoothing scales $20 < R < 23\,h^{-1}$ Mpc seems to be the most promising. In particular, by repeating this test for different redshifts and neutrino masses, we chose as our candidate scales $R = 22\,h^{-1}$ Mpc, $n = 2.1$.

define the neutrino contrast as

$$C = \frac{\mathrm{S/N}}{\max(\mathrm{S/N})} - \frac{\delta_{\rm combined}}{\max(\delta_{\rm combined})}. \tag{33}$$

Here we have normalized the signal/noise defined in equation (30) and the combined error defined in equation (32) to their respective maxima (on the considered grid) and we are interested in finding the regions where this contrast is dominated by the signal/noise, i.e. where $C(n, R) \sim 1$. In Fig. 6 we show the neutrino contrast on the (n, R) grid, for the simulation with $M_\nu = 0.17$ eV at redshift $z = 0.48551$.

We have repeated this analysis for the three massive neutrino simulations (with $M_\nu = 0.17,\ 0.30,\ 0.53$ eV) and for different redshifts, spanning the range from $z = 0.485\,51$ to $z = 2.050\,53$. Our conclusion is that the combination $R = 22\,h^{-1}$ Mpc, $n = 2.1$ is the most viable candidate for all these cosmologies and redshifts.

4.2 Likelihood

We aim at comparing measurements and predictions of the clustering ratio, in order to find the set of parameters of the model that maximizes the likelihood. We exploit the different dependence of measurements and predictions on the cosmological model. In particular, the measured value of the clustering ratio depends on the way we convert redshifts and angles into comoving distances, that depends on the total matter density $\Omega_{\rm m}$, on the dark energy fraction Ω_Λ and on the background expansion rate $H(z)$.

On the other hand, the theoretical prediction for the clustering ratio depends on the entire cosmological model and is therefore sensitive also to the value of the total neutrino mass M_ν.

We choose six baseline free parameters in our analysis, namely the baryon and cold dark matter density parameters $\Omega_{\rm b} h^2$ and $\Omega_{\rm cdm} h^2$, the Hubble parameter H_0, the optical depth at the recombination epoch τ, the amplitude of the scalar power spectrum at the pivotal scale $A_{\rm s}$ and the scalar spectral index $n_{\rm s}$. Moreover, we extend this parametrization with two additional free parameters, the total neutrino mass M_ν and the equation of state of the dark energy fluid w. The most general vector of parameters therefore is

$$\boldsymbol{p} = \{\Omega_{\rm b} h^2, \Omega_{\rm cdm} h^2, H_0, \tau, A_{\rm s}, n_{\rm s}, M_\nu, w\}.$$

We follow Bel & Marinoni (2014), who showed that the likelihood function of the clustering ratio (given a fixed set of parameters) is compatible with being a Gaussian. Therefore we will compute the logarithmic likelihood as $\ln \mathcal{L} = -\chi^2/2$ (apart from a normalization term) where

$$\chi^2(\boldsymbol{p}) = \sum_i \frac{(\eta_{R,i}(r) - \eta_{R,i}^{\rm th}(r))^2}{\sigma_{\eta_i}^2}, \tag{34}$$

where we neglect the covariance between the different redshift bins.

We account for the dependence of the measurements on the cosmological model assumed, induced by the cosmology-dependant conversion of redshifts into distances, whenever we compare measurements of the clustering ratio (obtained in the fiducial cosmology) to its predictions (in a generic cosmology). That is, when computing the likelihood for the set of parameters $\boldsymbol{\vartheta}$, we must keep in mind that the measured value has been computed in a different cosmology, the one with the fiducial set of parameters $\boldsymbol{\vartheta}^{\rm F}$.

We keep the measurements fixed in the fiducial cosmology and rescale the predictions accordingly. We consider that, due to Alcock–Paczyński effect, at same redshift and angular apertures we can associate different lengths depending on cosmology (Alcock & Paczyński 1979).

Our measurements depend on distances only through the smoothing scale R. This is because the correlation length is always expressed as a multiple of the smoothing scale, $r = nR$. This means that, since the measurement has been obtained in the fiducial cosmology using spheres of radius $R^{\rm F} = 22\,h^{-1}$Mpc, they need to be compared to predictions obtained in a generic cosmology using a smoothing length $R = \alpha R^{\rm F}$, where α is our Alcock–Paczyński correction.

We write the Alcock–Paczyński correction α as (Eisenstein et al. 2005)

$$\alpha = \left[\frac{E^{\rm F}(z)}{E(z)} \left(\frac{D_{\rm A}}{D_{\rm A}^{\rm F}} \right)^2 \right]^{1/3}, \tag{35}$$

where $E(z) \equiv H(z)/H_0$ is the normalized Hubble function and $D_{\rm A}$ the angular diameter distance. Therefore, we are going to compare

$$\eta^{\rm F,s}_{g,R}(nR) \equiv \eta_{\alpha R}(n\alpha R), \tag{36}$$

the left-hand side of equation (36) being the clustering ratio of galaxies measured in redshift space assuming the fiducial cosmology, while the right hand side is the predicted clustering ratio for matter in real space, rescaled to the fiducial cosmology to make it comparable with observations.

In order to efficiently explore the parameter space we have modified the public code COSMOMC (Lewis & Bridle 2002), adding a likelihood function that implements this procedure.

4.3 Constraints using SDSS data

We measure the clustering ratio in the 7th (Abazajian et al. 2009) and 12th (Alam et al. 2015) data release of the Sloan Digital Sky Survey (SDSS) by smoothing the galaxy distribution with spherical cells of radius R and counting the objects falling in each cell. We divide the sample into three redshift bins that have mean redshifts $\bar{z} = \{0.29, 0.42, 0.60\}$. The first redshift bin is extracted from the DR7 catalogue, while the two bins at higher redshift come from the DR12 catalogue, after removing the objects already present in the other bin.

To perform the count-in-cell procedure, we convert redshifts into distances, assuming a cosmology with $H_0 = 67\,{\rm km\,s^{-1}\,Mpc^{-1}}$, $\Omega_{\rm m} = 0.32$ and in which we fix the geometry of the universe to be flat, $\Omega_k = 0$, forcing $\Omega_\Lambda = 1 - \Omega_{\rm r} - \Omega_{\rm m}$. Therefore, this is to be considered our fiducial cosmology. We compute the clustering ratio using the estimators presented in Section 2.1, employing our optimized smoothing size and correlation length, $R = 22\,h^{-1}$Mpc and $r = 2.1\,R$. Our measurements of the clustering ratio in each redshift bin are

$$\begin{aligned} &\text{at } 0.15 \le z \le 0.43, \quad \eta_{g,R}(r) = 0.0945 \pm 0.0067,\\ &\text{at } 0.30 \le z \le 0.53, \quad \eta_{g,R}(r) = 0.0914 \pm 0.0055,\\ &\text{at } 0.53 \le z \le 0.67, \quad \eta_{g,R}(r) = 0.1070 \pm 0.0110. \end{aligned}$$

Details on the computation of the clustering ratio and its errors in the SDSS catalogue can be found in Bel et al. (2015), where, though, measurements are performed assuming a different fiducial cosmology.

In Fig. 7 we show, for some relevant parameters, the joint posterior distribution obtained fitting at the same time the *Planck* temperature and polarization data and the clustering ratio measurements in SDSS DR7 and DR12, leaving free to vary the six baseline parameters and the total neutrino mass M_ν. Already by eye, adding the clustering ratio to the CMB information does not seem to improve much the upper bound of the total neutrino mass parameter. In general, the most significant improvement seems to occur on the constraint of the cold dark matter density parameter.

Moreover, we have also checked how constraints change when we leave the equation of state of dark energy, w, as an additional free parameter. As a matter of fact, w is known to be strongly

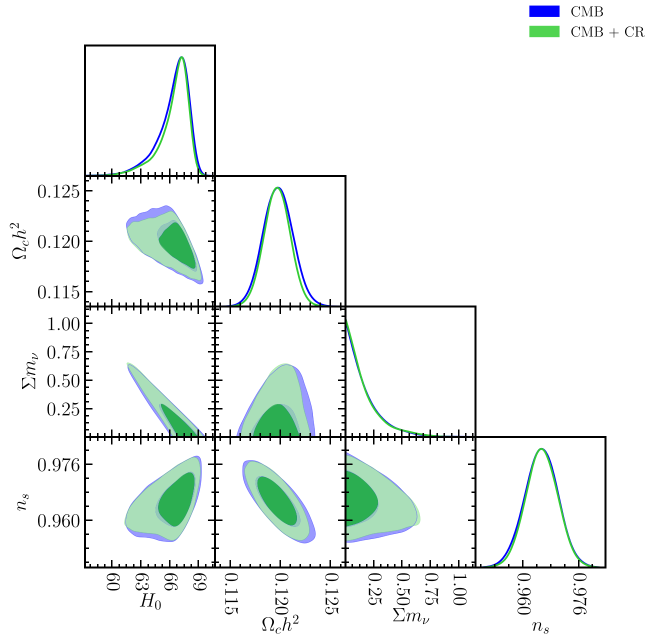

Figure 7. Joint posterior distribution obtained using *Planck* temperature and polarization data and the clustering ratio measured in SDSS DR7 and 12. We fit a cosmological model with seven free parameters, the six baseline parameters of *Planck* and the neutrino total mass, but here only four of them are shown.

degenerate with the other parameters of the model, when only CMB data are used. In general, we need information from a geometrical probe sensitive to the late time universe in order to force physical solutions. Fig. 8 shows that the clustering ratio is indeed able to break such degeneracy.

Also the combination of other cosmological probes can help breaking degeneracies and tightening constraints. For this reason we compare the constraining power of the clustering ratio to that of two other observables, the fit of the BAO peak in the correlation function measured by the BOSS collaboration in the DR11 CMASS and LOWZ data sets (Anderson et al. 2014) and the lensing of the CMB signal due to the intervening matter distribution between the last scattering surface and us, where the amplitude of the lensing potential, $A_{\rm L}$, has been kept fixed to 1 (Planck Collaboration XI 2016).

In the first part of Table 4 we show the mean, 68 per cent and 95 per cent levels obtained for the different parameters combining the likelihoods presented above. To better show the behaviour of the clustering ratio with respect to the other probes considered, in Figs 9 and 10, we focus particularly on the parameters w, M_ν, and H_0.

In general, adding the clustering ratio considerably improves on the parameter constraints obtained with CMB data alone, especially when also w is free to vary. In particular, the clustering ratio is able to break the degeneracy between w and the other cosmological parameters, that affects the constraints drawn with the sole CMB data. The clustering ratio does not, however, seem to improve much the constraint on the M_ν parameter, especially when compared to probes such as the CMB lensing and the BAO peak position.

The clustering ratio proves to be extremely sensitive to the cold dark matter fraction $\Omega_{\rm cdm}h^2$, as adding the clustering ratio to the CMB analysis results in a 12 per cent improvement on the

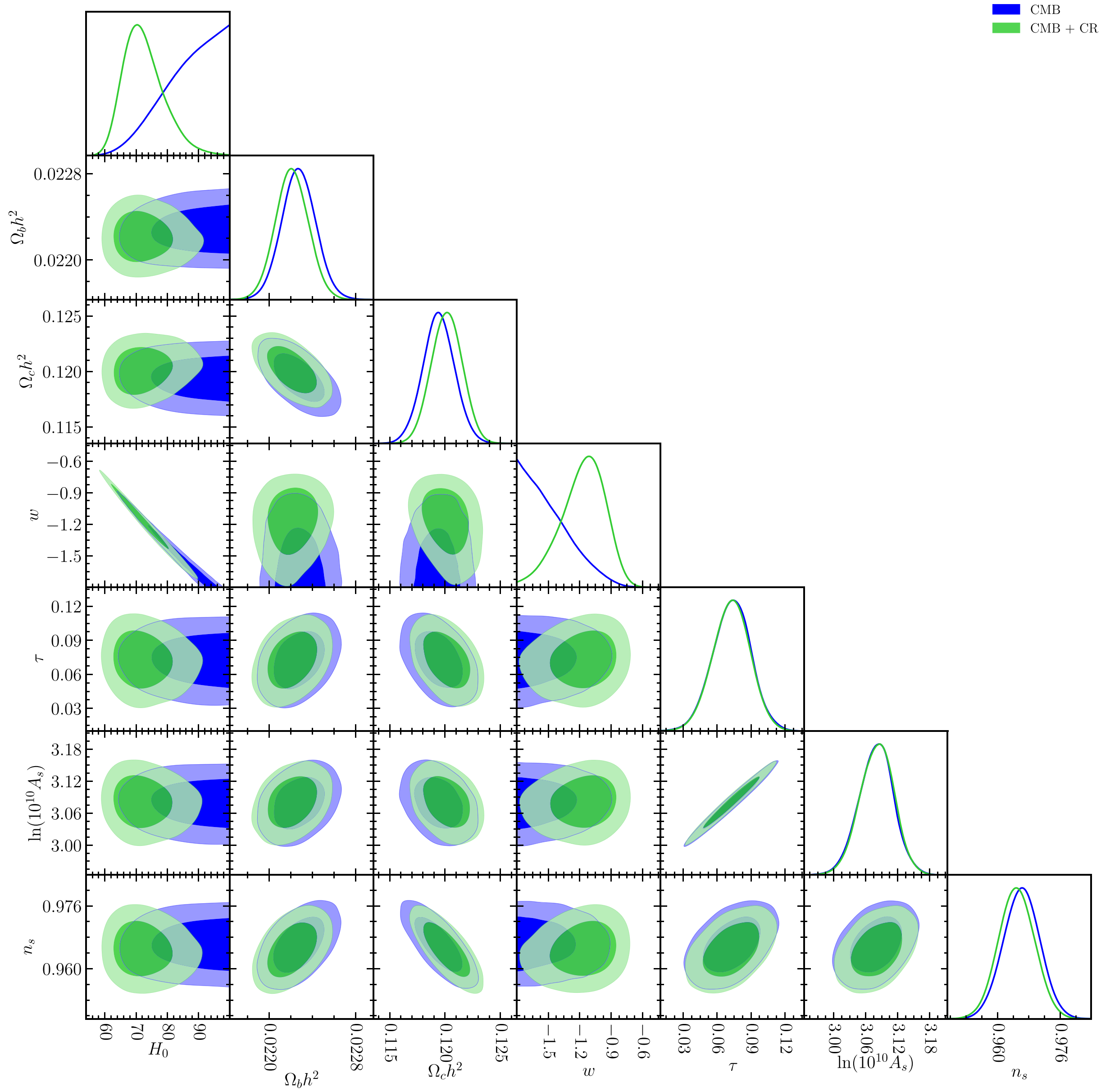

Figure 8. Joint posterior distribution obtained employing CMB temperature and polarization data from *Planck* and the clustering ratio measurements from SDSS DR7 and DR12 catalogues. Besides the six standard parameters of the model, also the equation of state of dark energy is left free.

95 per cent confidence level, which goes from $0.119\,78 \pm 0.002\,91$ (obtained using *Planck* data alone) to $0.119\,72 \pm 0.002\,55$.

To improve our understanding of the results presented in the previous section, we investigate how well the clustering ratio allows us to recover a certain known cosmology.

To this purpose, we use the measurements of the clustering ratio in one of the DEMNUni simulations, the one with $M_\nu = 0.17$ eV, which represents the closest value to the current available constraints on the neutrino total mass. The clustering ratio is measured in the simulation at the same redshifts, and with the same binning, as in the SDSS data. The error on each measurement in the simulation is assumed to be the same as SDSS measurements.

The likelihood using the CMB data is computed in this case fixing the bestfits to the values of the parameters in the cosmology of the simulation, and employing the covariance matrix contained in the publicly available *Planck* data release.

The posterior distribution obtained with this procedure is shown in Fig. 11, while the second part of Table 4 summarizes the improvements on the constraints on the parameters that we obtain adding the clustering ratio. We correctly recover the bestfits of our known cosmology, with errors comparable with the true ones. We conclude that the reason why we did not achieve a significant improvement on the constraint on the total neutrino mass using the SDSS data resides in the fact that the clustering ratio requires smaller error bars to be effective in constraining such parameter. We can therefore expect that, with upcoming, large galaxy redshift surveys, the clustering ratio will reach a larger constraining power.

Table 4. Mean, 68 per cent, and 95 per cent levels of the marginalized posterior distributions. In the first part of the table the data sets of *Planck*'s CMB temperature and polarization anisotropies, BOSS measurement of the BAO peak, and *Planck*'s CMB lensing signal are used in combination with the clustering ratio measured in the SDSS DR7+12 sample. In the second part of the table bestfits have been fixed to the ones of the fiducial cosmology, errors for *Planck* are obtained from the publicly available *Planck* parameter covariance matrix and error for the clustering ratio are the ones measured in SDSS DR7 and DR12. Finally, in the last part of the table, bestfits have been fixed to the ones of the fiducial cosmology, errors for *Planck* are obtained from the publicly available *Planck* parameter covariance matrix and errors for the clustering ratio are the ones predicted for a Euclid-like galaxy survey, following the procedure described in the text.

	$\Omega_b h^2$			$\Omega_c h^2$			τ			M_ν		
Pl (fixed w)	0.022 22	± 0.000 17	± 0.000 33	0.119 78	± 0.001 47	± 0.002 91	0.078 51	± 0.017 13	± 0.033 55	0.167 22	<0.191 50	<0.494 02
Pl + CR (fixed w)	0.022 22	± 0.000 16	± 0.000 31	0.119 72	± 0.001 28	± 0.002 55	0.078 01	± 0.017 44	± 0.033 30	0.157 95	<0.180 88	<0.478 35
Pl	0.022 22	± 0.000 16	± 0.000 34	0.119 71	± 0.001 42	± 0.002 81	0.077 37	± 0.017 93	± 0.034 83	0.221 53	<0.266 98	<0.608 51
Pl + CR	0.022 16	± 0.000 17	± 0.000 33	0.120 42	± 0.001 49	± 0.002 90	0.074 69	± 0.017 54	± 0.034 03	0.203 04	<0.245 10	<0.530 81
Pl + CLens	0.022 17	± 0.000 17	± 0.000 35	0.119 67	± 0.001 53	± 0.002 99	0.069 27	± 0.017 49	± 0.034 20	0.328 82	± 0.197 11	<0.672 19
Pl + BAO	0.022 25	± 0.000 15	± 0.000 30	0.119 49	± 0.001 34	± 0.002 63	0.077 28	± 0.017 05	± 0.033 04	0.115 71	<0.142 35	<0.304 23
Pl + CLens + CR	0.022 13	± 0.000 16	± 0.000 32	0.120 26	± 0.001 45	± 0.002 88	0.069 09	± 0.016 81	± 0.032 37	0.294 40	± 0.175 24	<0.594 71
Pl + BAO +CR	0.022 23	± 0.000 15	± 0.000 30	0.119 65	± 0.001 32	± 0.002 61	0.077 31	± 0.016 66	± 0.031 47	0.108 44	<0.131 43	<0.283 39
	w			$\ln(10^{10}A_s)$			n_s			H_0		
Pl (fixed w)	− 1.000 00	–	–	3.091 67	± 0.033 32	± 0.065 10	0.965 31	± 0.004 78	± 0.009 51	66.362 05	$^{+1.93320}_{-0.79827}$	± 3.145 33
Pl + CR (fixed w)	− 1.000 00	–	–	3.090 42	± 0.033 75	± 0.064 97	0.965 50	± 0.004 56	± 0.009 06	66.470 15	$^{+1.72753}_{-0.68157}$	± 2.934 40
Pl	− 1.686 15	± 0.295 43	± 0.592 85	3.088 81	± 0.034 90	± 0.067 51	0.965 00	± 0.004 73	± 0.009 53	86.914 46	$^{+12.41268}_{-4.70920}$	± 15.599 71
Pl + CR	− 1.253 76	± 0.242 54	± 0.520 00	3.085 37	± 0.033 68	± 0.065 50	0.963 89	± 0.004 87	± 0.009 67	73.042 63	± 6.833 17	± 14.513 62
Pl + CLens	− 1.676 28	± 0.359 84	± 0.667 50	3.071 48	± 0.033 87	± 0.065 78	0.964 52	± 0.005 02	± 0.009 78	84.624 50	$^{+14.64438}_{-5.54025}$	± 16.855 12
Pl + BAO	− 1.058 67	± 0.079 59	± 0.163 54	3.088 46	± 0.033 05	± 0.064 28	0.966 12	± 0.004 51	± 0.008 86	68.600 48	± 1.673 61	± 3.369 35
Pl + CLens + CR	− 1.222 98	± 0.239 81	± 0.512 34	3.072 59	± 0.031 89	± 0.061 76	0.963 85	± 0.004 93	± 0.009 46	71.084 54	± 6.310 34	± 13.487 06
Pl + BAO + CR	− 1.052 67	± 0.077 49	± 0.157 31	3.089 03	± 0.03209	± 0.060 98	0.965 95	± 0.004 53	± 0.008 88	68.421 43	± 1.636 37	± 3.264 16
	$\Omega_b h2$			$\Omega_c h^2$			τ			M_ν		
Pl (fixed w)	0.022 44	± 0.000 16	± 0.00034	0.119 48	± 0.001 57	± 0.003 14	0.093 32	± 0.016 44	± 0.032 91	0.204 77	<0.264 41	<0.429 93
Pl + CR (fixed w)	0.022 42	± 0.000 15	± 0.00030	0.119 50	± 0.001 36	± 0.002 65	0.091 99	± 0.016 59	± 0.032 29	0.208 43	± 0.119 09	<0.410 13
	w			$\ln(10^{10}A_s)$			n_s			H_0		
Pl (fixed w)	− 1.000 00	–	–	3.058 93	± 0.031 69	± 0.063 81	0.959 37	± 0.005 18	± 0.010 15	66.651 75	± 1.436 57	± 2.673 94
Pl + CR (fixed w)	− 1.000 00	–	–	3.056 20	± 0.032 64	± 0.064 22	0.959 69	± 0.004 58	± 0.009 18	66.603 47	± 1.232 52	± 2.418 51
	$\Omega_b h^2$			$\Omega_c h^2$			τ			M_ν		
Pl (fixed w)	0.022 43	± 0.000 16	± 0.000 31	0.119 42	± 0.001 46	± 0.002 90	0.093 35	± 0.017 47	± 0.034 45	0.205 13	± 0.123 82	<0.431 57
Pl + CR (fixed w)	0.022 45	± 0.000 13	± 0.000 26	0.119 26	± 0.000 84	± 0.001 67	0.094 22	± 0.016 55	± 0.032 98	0.177 49	± 0.111 33	<0.376 93
	w			$\ln(10^{10}A_s)$			n_s			H_0		
Pl (fixed w)	− 1.000 00	–	–	3.058 59	± 0.033 78	± 0.066 70	0.959 83	± 0.004 91	± 0.009 64	66.665 88	± 1.384 64	± 2.629 98
Pl + CR (fixed w)	− 1.000 00	–	–	3.060 08	± 0.032 62	± 0.064 76	0.960 46	± 0.004 43	± 0.008 54	66.982 61	± 1.122 63	± 2.183 65

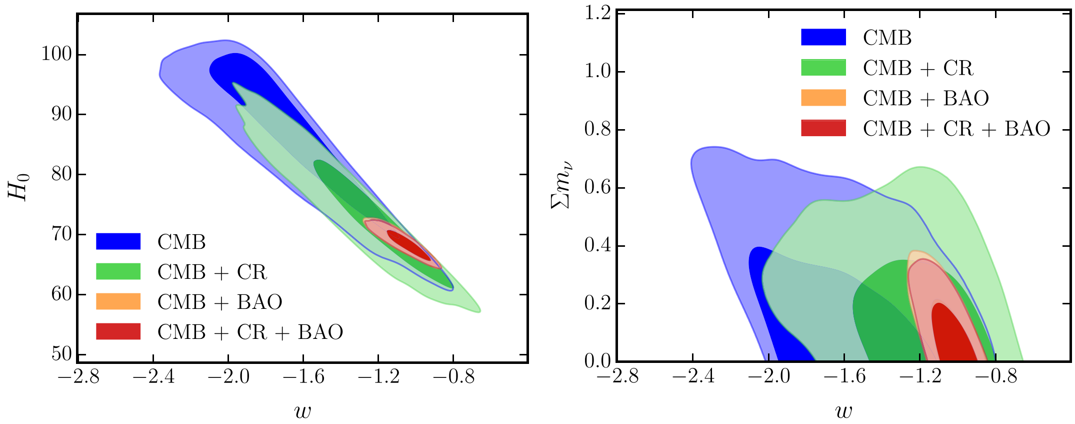

Figure 9. Left: Degeneracy between the equation of state of dark energy, w, and the Hubble parameter today H_0. Right: Degeneracy between w and the total neutrino mass M_ν. The considered likelihoods are computed using *Planck* data alone, as well as its combinations with the clustering ratio measured in SDSS DR7 and 12, the *BAO position* from SDSS DR11, or both.

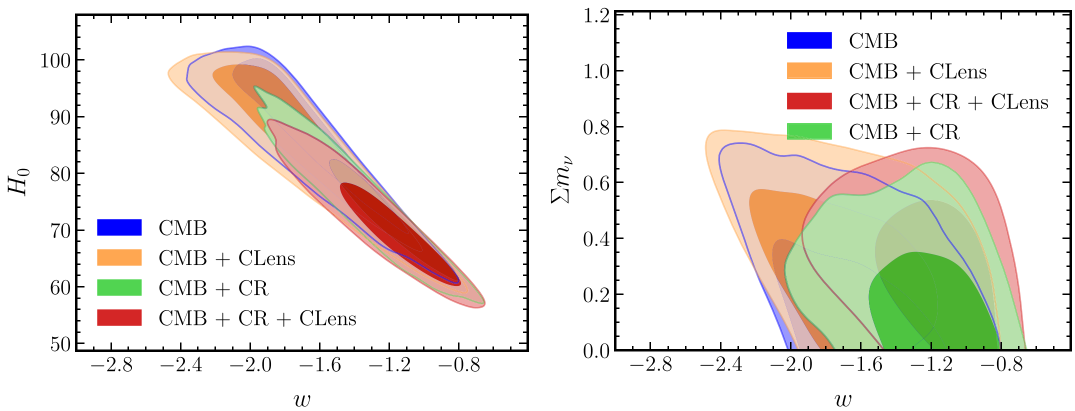

Figure 10. Left: Degeneracy between the equation of state of dark energy, w, and the Hubble parameter today H_0. Right: Degeneracy between w and the total neutrino mass M_ν. The considered likelihoods are computed using *Planck* data alone, as well as its combinations with the clustering ratio measured in SDSS DR7 and 12, *CMB-lensing*, or both.

We test such an hypothesis in the next section, analysing the clustering ratio expected for a Euclid-like galaxy redshift survey, in combination with CMB data.

5 FORECASTS FOR A EUCLID-LIKE GALAXY REDSHIFT SURVEY

In order to forecast the constraining power of the clustering ratio, expected from a future, Euclid-like galaxy redshift survey, we construct the synthetic clustering ratio data in the following way:

(i) We imagine to have 14 redshift bins, from $z = 0.7$ to $z = 2$, with $\Delta z = 0.1$.

(ii) In each redshift bin, the synthetic measurement of the clustering ratio is given by the predicted clustering ratio (computed using a Boltzmann code), to which we add a small random noise (within 1 standard deviation).

(iii) We measure the errors (at the same redshifts) in the DEMNUni simulations; the errors in the simulations are then rescaled, according to the operative formula presented below, to match the volume and number density of our Euclid-like survey.

The relative error on the clustering ratio depends on the volume and number density of the sample, and can be parametrized, following Bel et al. (2015), as

$$\frac{\delta\eta}{\eta} = A V^{-1/2} \exp\left\{0.14\left[\ln\rho - \frac{\ln^2\rho}{2\ln(0.02)}\right]\right\}, \quad (37)$$

where V is the volume expressed in h^{-3} Mpc^3, ρ is the object number density in h^3 Mpc^{-3} and A is a normalization factor computed with the reference volume and number density.

We use these data to explore the posterior distribution of the parameters of the model. The results are shown in Fig. 12, and the constraints are shown in the last part of Table 4.

The obtained best fits in all cases are compatible within one standard deviation with the fiducial values that we assumed. In general, with these synthetic data, there is a much larger improvement on the constraints of all the parameters. The neutrino total mass parameter goes from a 95 per cent upper limit of <0.431 eV obtained using the *Planck* covariance matrix alone, to <0.377 eV when the information of the clustering ratio is added to the analysis (∼14 per cent improvement). Most notably, the 95 per cent limits on the cold dark matter density parameter improve by over 40 per cent, going from $\Omega_{\rm cdm}h^2 = 0.119\,42 \pm 0.002\,90$ using *Planck* alone, to $\Omega_{\rm cdm}h^2 = 0.119\,26 \pm 0.001\,67$ by adding the clustering ratio. Also the spectral index $n_{\rm s}$ goes from $0.959\,83 \pm 0.009\,64$ to $0.960\,46 \pm 0.008\,54$ (10 per cent improvement with respect to *Planck* alone) and the constraint on the Hubble constant H_0 goes

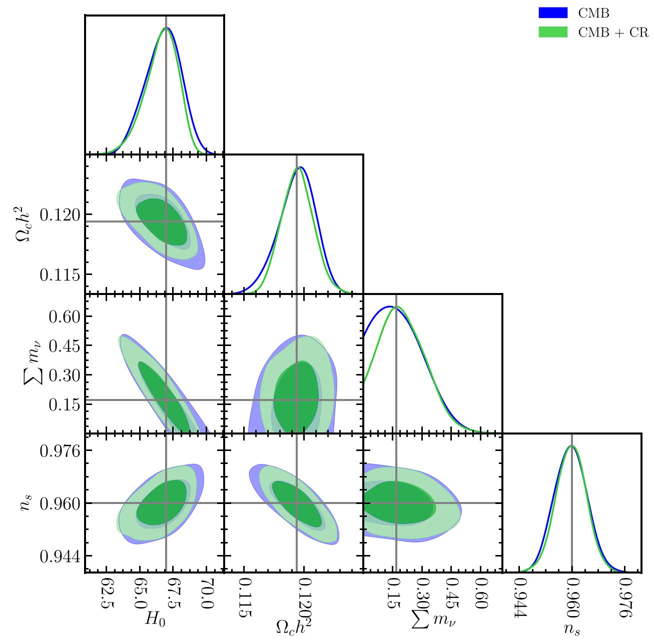

Figure 11. Joint posterior distribution obtained using *Planck* temperature and polarization data combined with clustering ratio measurements. Bestfits here are fixed, errors for *Planck* come from the publicly available covariance matrix, errors on clustering ratio measurements have been computed in the case of SDSS DR7 and DR12 data. Four of the seven free parameters are shown.

from 66.665 88 $\pm$ 1.384 64 to 66.982 61 $\pm$ 1.122 63 (20 per cent improvement over *Planck* alone).

This means that, when new data, covering a larger volume, will be available, clustering ratio measurements are expected to contribute with a significant improvement on the constraints on the parameters of the cosmological model.

We also note that, as more different observations are carried out, it becomes very interesting to enhance the constraining power of the clustering ratio also combining its measurements in different data sets. This can be easily done since the clustering ratio is a single measurement, thus scarcely dependent on the survey geometry.

6 SUMMARY AND CONCLUSION

Neutrino effects are being increasingly included in cosmological investigations, becoming in fact part of the standard cosmological model. Thanks to these investigations, the description of the statistical properties of the universe is gaining the precision required by forthcoming experiments and, at the same time, neutrino physics gains tighter constraints.

In this work we have considered the clustering ratio, an observable defined as the ratio between the smoothed correlation function and variance of a distribution, and extended its range of applicability to cosmologies that include a massive neutrino component. As a matter of fact, the clustering ratio, which has already been tested in ΛCDM cosmologies including only massless neutrinos, is unbiased and independent from redshift-space distortions on linear scales. As massive neutrinos introduce characteristic scale dependencies in the clustering of galaxies (and matter), such peculiar properties of the clustering ratio needed to be confirmed (or denied) in this cosmological framework.

We divided our analysis into two steps: first, we studied the properties of the clustering ratio in simulations that include massive neutrinos; afterwards, we used the clustering ratio to compute the likelihood of the parameters of the cosmological model, using both real data and forecasts of future data.

In the first part of this work, we employed the DEMNUni simulations to test the clustering ratio in the presence of massive neutrinos. These are the largest available simulations that include massive neutrinos as a separate particle species along with cold dark matter. We computed the clustering ratio using different tracers (dark matter FoF haloes and spherical overdensities), divided into different mass bins (spanning the interval from $\sim 6 \times 10^{11}$ to $\gtrsim 10^{14}\, h^{-1}\, \mathrm{M}_{\odot}$), and we explore different choices of neutrino mass ($M_\nu = \{0, 0.17, 0.3, 0.53\}$ eV) in real and redshift space.

From such analysis we conclude that the properties of the clustering ratio hold also in cosmologies with massive neutrinos. In particular its main property, the fact that the galaxy clustering ratio in redshift space is directly comparable to the clustering ratio predicted for matter in real space on a range of linear scales, is proven valid.

We have therefore moved to employing the clustering ratio as a cosmological probe to find the set of parameters of the model that maximizes the likelihood function, given a set of data. We have used the data from the SDSS DR7+DR12 catalogue. We have computed the clustering ratio in three redshift bins and used these measurements in combination with the temperature and polarization anisotropies of the CMB measured by the *Planck* satellite to explore the likelihood in parameter space with an MCMC approach. We find that the clustering ratio is able to break the degeneracy, present in the CMB data alone, between the equation of state of dark matter, *w*, and the other parameters. Moreover it improves the 95 per cent limit on the CDM density parameter by $\sim$12 per cent, going from 0.119 78 $\pm$ 0.002 91 (obtained using *Planck* data alone) to 0.119 72 $\pm$ 0.002 55. However, we do not find an appreciable improvement in the constraint on the neutrino total mass.

By analysing simulations we conclude that we blame such lack of improvement on the statistical errors, which, with current data, are not yet competitive enough. We have therefore tested the constraining power of the clustering ratio using the error bars expected from a Euclid-like galaxy survey.

In this case we find that the clustering ratio greatly improves the constraint on the CDM density parameter, shrinking the 95 per cent limit from a typical error of $\pm$0.002 90 (using CMB data alone) to $\pm$0.001 67, which corresponds to a $\sim$40 per cent improvement. Also the constraints on all the other free parameters improve, for example the 95 per cent limit on the Hubble parameter H_0 shrinks by 20 per cent (from $\pm$2.6 to $\pm$2.2). Finally, it is also able to improve the 95 per cent upper bound on the total neutrino mass by $\sim$14 per cent, going from $<$0.432 to $<$0.377 eV.

In conclusion, the clustering ratio appears to be a valuable probe to constrain the parameters of the cosmological model, especially with upcoming large galaxy redshift surveys. Being easy to model and measure, it provides us with a powerful tool to complement other approaches to galaxy clustering analysis, such as the measurements of the galaxy correlation function or power spectrum. Moreover, we note that, given the simplicity of combining the clustering ratio measured in different surveys, we expect its true constraining power to emerge when it will be measured in a number of different data sets.

ACKNOWLEDGEMENTS

LG, JB, CC, and JD acknowledge financial support from the European Research Council through the Darklight Advanced

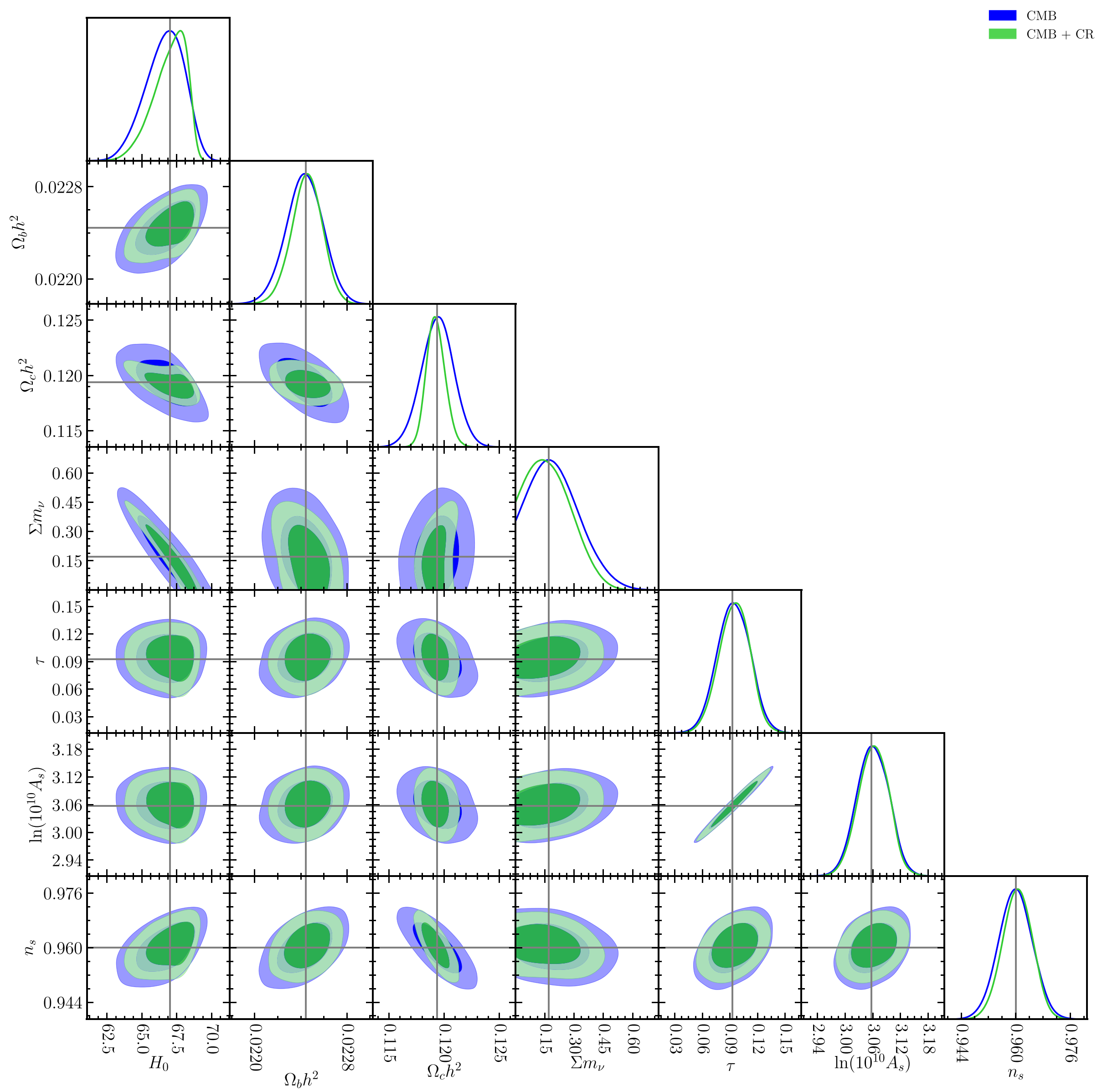

Figure 12. Joint posterior distribution obtained combining *Planck* temperature and polarization data together with the clustering ratio measured in a Euclid-like galaxy survey. For CMB data, errors come from the publicly available covariance matrix, for clustering ratio measurements errors have been obtained from the DEMNUni simulations and rescaled to match the volume and number density of the mock Euclid survey.

Research Grant (n. 291521). CC acknowledges the support from the grant MIUR PRIN 2015 ‘Cosmology and Fundamental Physics: illuminating the Dark Universe with Euclid’. The DEMNUni simulations were carried out at the Tier-0 IBM BG/Q machine, *Fermi*, of the Centro Interuniversitario del Nord-Est per il Calcolo Elettronico (CINECA, Bologna, Italy), via the five million cpu-hrs budget provided by the Italian SuperComputing Resource Allocation (ISCRA) to the class-A proposal entitled ‘The Dark Energy and Massive-Neutrino Universe’.

REFERENCES

Abazajian K. N. et al., 2009, ApJS, 182, 543
Alam S. et al., 2015, ApJS, 219, 12
Alcock C., Paczyński B., 1979, Nature, 281, 358
Anderson L. et al., 2014, MNRAS, 441, 24
Archidiacono M., Brinckmann T., Lesgourgues J., Poulin V., 2017, J. Cosmol. Astropart. Phys., 2, 052
Bel J., Marinoni C., 2012, MNRAS, 424, 971
Bel J., Marinoni C., 2014, A&A, 563, A36
Bel J. et al., 2014, A&A, 563, A37
Bel J., Hoffmann K., Gaztañaga E., 2015, MNRAS, 453, 259
Bernardeau F., Colombi S., Gaztañaga E., Scoccimarro R., 2002, Phys. Rept., 367, 1
Blas D., Garny M., Konstandin T., Lesgourgues J., 2014, J. Cosmol. Astropart. Phys., 11, 039
Bonn J., Eitel K., Glück F., Sevilla-Sanchez D., Titov N., Blaum K., 2011, Phys. Lett. B, 703, 310
Carbone C., Verde L., Wang Y., Cimatti A., 2011b, J. Cosmol. Astropart. Phys., 3, 030
Carbone C., Mangilli A., Verde L., 2011a, J. Cosmol. Astropart. Phys., 9, 028
Carbone C., Petkova M., Dolag K., 2016, J. Cosmol. Astropart. Phys., 7, 034

Casas-Miranda R., Mo H. J., Sheth R. K., Boerner G., 2002, MNRAS, 333, 730
Castorina E., Carbone C., Bel J., Sefusatti E., Dolag K., 2015, J. Cosmol. Astropart. Phys., 7, 043
Chan K. C., Scoccimarro R., Sheth R. K., 2012, Phys. Rev. D, 85, 083509
Cuesta A. J., Niro V., Verde L., 2016, Phys. Dark Universe, 13, 77
Desjacques V., Jeong D., Schmidt F., 2016, preprint (arXiv:1611.09787)
Di Valentino E., Melchiorri A., 2014, Phys. Rev. D, 90, 083531
Eisenstein D. J. et al., 2005, ApJ, 633, 560
Esteban I., Gonzalez-Garcia M. C., Maltoni M., Martinez-Soler I., Schwetz T., 2017, J. High Energy Phys., 1, 87
Forero D. V., Tórtola M., Valle J. W. F., 2014, Phys. Rev. D, 90, 093006
Fry J. N., 1984, ApJ, 279, 499
Fry J. N., Gaztanaga E., 1993, ApJ, 413, 447
Gonzalez-Garcia M. C., Maltoni M., Salvado J., Schwetz T., 2012, J. High Energy Phys., 12, 123
Gonzalez-Garcia M. C., Maltoni M., Schwetz T., 2014, J. High Energy Phys., 11, 52
Kaiser N., 1987, MNRAS, 227, 1
Kraus C. et al., 2005, Eur. Phys. J. C, 40, 447
Lesgourgues J., Pastor S., 2006, Phys. Rept., 429, 307
Lesgourgues J., Pastor S., 2012, preprint (arXiv: e-prints 1212.6154)
Lesgourgues J., Pastor S., 2014, New J. Phys., 16, 065002
Lewis A., Bridle S., 2002, Phys. Rev. D, 66, 103511
Manera M., Gaztañaga E., 2011, MNRAS, 415, 383
Mo H. J., White S. D. M., 1996, MNRAS, 282, 347
Planck Collaboration XI, 2016, A&A, 594, A11
Sheth R. K., Lemson G., 1999, MNRAS, 304, 767
Shoji M., Komatsu E., 2010, Phys. Rev. D, 82, 089901
Somerville R. S., Lemson G., Sigad Y., Dekel A., Kauffmann G., White S. D. M., 2001, MNRAS, 320, 289
Springel V., 2005, MNRAS, 364, 1105
Springel V., White S. D. M., Tormen G., Kauffmann G., 2001, MNRAS, 328, 726
Vagnozzi S., Giusarma E., Mena O., Freese K., Gerbino M., Ho S., Lattanzi M., 2017, Phys. Rev. D, 96, 123503
Viel M., Haehnelt M. G., Springel V., 2010, J. Cosmol. Astropart. Phys., 6, 015
Zennaro M., Bel J., Villaescusa-Navarro F., Carbone C., Sefusatti E., Guzzo L., 2017, MNRAS, 466, 3244

This paper has been typeset from a TEX/LATEX file prepared by the author.